Pergamon

Int. J. Heat Mass Transfer. Vol. 38, No. 3, pp. 445–453, 1995

0017-9310/95 $9.50+0.00

0017-9310(94)00181-2

Axial development of interfacial area and void concentration profiles measured by double-sensor probe method

W. H. LEUNG, S. T. REVANKAR, Y. ISHII† and M. ISHII‡

School of Nuclear Engineering, Purdue University, West Lafayette, IN 47906, U.S.A.

(*Received* 19 *July* 1993 *and in final form* 7 *June* 1994)

Abstract—Interfacial area concentration is an important parameter in modeling the interfacial transfer terms in the two-fluid model. In this paper, the local geometric and statistical characteristics of upward co-current dispersed bubbly flow in a pipe have been studied both at the entrance ($L/D = 8$) and at a region far away from the entrance ($L/D = 60$). The test section was a 5.08 cm i.d. and 375 cm long Lucite pipe. Four liquid flow rates ranging from 0.1 to 1.0 m s^{-1} were used in combination with four different gas injection rates ranging from 0.02 to 0.1 m s^{-1}. A double-sensor probe was employed to measure the radial profiles of void fraction, interfacial area concentration, Sauter mean diameter, bubble velocity and bubble frequency. The wall peak of the void fraction profile was established within a short distance from the entrance. The flow characteristics changed very little from the entrance region to the fully developed region except for the flow case of $j_l = 0.1$ m s^{-1}. The area averaged flow quantities were also presented.

1. INTRODUCTION

The two-fluid model is the most detailed description of a two-phase flow system because it describes the phases separately in terms of the conservation equations in mass, momentum, and energy. The interactions between the two phases are modeled by the interfacial transfer terms. Due to the basic nature of this formulation, it requires a detailed knowledge of the interfacial structure, particularly of the interfacial area concentration. The local instantaneous formulation of the two-phase flow is difficult to apply because it contains information on the fast fluctuating fields and the discontinuities at the interfaces. In order to avoid a lengthy description of microscopic characteristics of the two-phase flow system, the average model is often used to describe a two-phase system. Various methods of formulating the two-fluid model have been studied by Ishii [1]. The average form of the conservation equations removes the discontinuities at the interfaces and gives the averaged macroscopic interfacial transport description. The choice of the averaging method depends on the problem to be solved and the necessary constitutive relations which should be developed from the experimental data. Thus, the averaging method and the measurement technique should be consistent. For example, if a local probe records the flow field fluctuation in the time domain, then measurements are useful in the local time average two-fluid model which is a practical technique to characterize the local flow field in two-phase flow.

In dispersed two-phase flow, the momentum transfer can be modeled as the total surface forces imposing upon the fluid particles by the continuum. By neglecting the lift force and the diffusion force, the general drag force for the dispersed phase is given in a simple form [2]:

$$\mathbf{M}_{id} = \alpha_d \frac{\mathbf{F}_D}{B_d} + \alpha_d \frac{\mathbf{F}_V}{B_d} + \frac{9}{2}\frac{\alpha_d}{r_d}\sqrt{\frac{\rho_c \mu_m}{\pi}} \int_t \frac{D_d}{D\xi}(\mathbf{v}_d - \mathbf{v}_c)\frac{d\xi}{\sqrt{t-\xi}}, \quad (1)$$

where $\mathbf{F}_D$, B_d, $\mathbf{F}_V$ and μ_m are the standard drag force, volume of a typical particle, virtual mass force and mixture viscosity, respectively. The last term is the Basset force which is a force imposed on a fluid particle due to the developing boundary layer at the interface. The standard drag force acting on the dispersed phase can be expressed as [2]:

$$\alpha_d \frac{\mathbf{F}_D}{B_d} = -a_i\left[\frac{C_D}{4}\left(\frac{r_{Sm}}{r_D}\right)\frac{\rho_c \mathbf{v}_r |\mathbf{v}_r|}{2}\right], \quad (2)$$

where $\mathbf{v}_r$ is the relative velocity between the dispersed and the continuous phase. The two radii are the Sauter mean radius, r_{Sm}, and the drag radius, r_D, and their ratio denotes the shape factor. They are defined as [2]:

$$r_{Sm} = \frac{3B_d}{A_i} \quad r_D = \frac{3B_d}{4A_d}, \quad (3)$$

where A_i and A_d are the surface area and projected

†Present address: Energy Research Laboratory, Hitachi Ltd., 1168 Moriyama-cho, Hitachi-shi Ibaraki-ban, 316 Japan.

‡Author to whom correspondence should be addressed.

NOMENCLATURE

$\bar{a}_i^t$ time average interfacial area concentration
A_d projected area of a typical particle
B_d volume of typical particle
C_0 distribution parameter
$\mathbf{F}_D$ standard drag force
$\mathbf{F}_V$ virtual mass force
j_g, j_l superficial velocity of gas and liquid
N number of bubbles a point per unit time
r_d drag radius of typical particle
r_{Sm} Sauter mean radius
t_j time when jth interface passes the probe
$\mathbf{v}_j$ velocity of jth interface
$\mathbf{v}_{jzj}$ z component of interfacial velocity
$\mathbf{v}_{szj}$ passing velocity of jth interface through double probe in z-direction.

Greek symbols

α void fraction of gas phase
α_0 limiting value of angle of α_j
α_j angle between n_j and projection of n_j into x–y-plane
β_j angle between projection of n_j into x–y-plane and y-axis
Δs spacing between tip and rear sensor of double probe
Δt_j time difference between an interface hitting the upstream and downstream sensor
$\Delta\tau_j$ resident time of the sensor in jth bubble
μ_j angle between v_j and projection into x–y-plane
ν_j angle between projection of v_j into x–y-plane and y-axis
ξ_j angle between n_j and n_s
σ_z, σ_{sz} rms of fluctuating components of v_{izj}, v_{sz}
ϕ angle between n_j and v_j
Ω time interval of averaging over sampling.

Subscripts

c continuous phase
d dispersed phase
df downstream sensor signal fall point
dr downstream sensor signal rise point
i value at an interface
j the jth interface
l liquid phase
g gas phase
uf upstream signal fall point
ur upstream sensor signal rise point.

Operators

— arithmetic mean
$\langle\rangle$ area averaging.

area of a typical particle. This indicates that the drag force per unit volume of mixture is proportional to the interfacial area concentration and drag coefficient.

The interfacial energy transport is characterized by the macroscopic jump of the enthalpy. If the mechanical energy transfer terms can be neglected, the enthalpy interfacial transfer condition indicates that the constitutive relation for Γ_k is equivalent to specifying the heat flux at the interface for both phases. This greatly simplifies the development of the algebraic model of the interfacial energy transfer terms. By introducing the mean mass transfer per unit area, m_k, the total mass flux can be defined as $\Gamma_k = a_i m_k$, and the interfacial energy transfer term can be written as:

$$\Gamma_k H_{ki} + q''_{ki} a_i = a_i (m_k H_{ki} + q''_{ki}). \quad (4)$$

The heat flux at the interface should be modeled by using the temperature gradient at the interface as the driving force. Hence, it can be expressed as $q''_{ki} = h_{ik}(T_i - T_k)$, where T_i and T_k are the interfacial and bulk temperatures based on the mean enthalpy.

In view of equations (2) and (4), the general form of the interfacial transfer terms can be written as a product of the interfacial area concentration, a_i, and the driving force:

(INTERFACIAL TRANSFER TERM)

$$= a_i \times (\text{DRIVING FORCE}). \quad (5)$$

The importance of the interfacial area concentration, a_i, in developing the constitutive relations for these terms is evident. It is essential to make a conceptual distinction between the effects of a_i and the driving force. The interfacial transfer of mass, momentum and energy are directly proportional to the available interfacial area and the potential difference between the phases.

Furthermore, the local distribution of the dispersed phase is affected by the concentration of interfacial area. Recently, Serizawa *et al.* [3] studied the bubble size effect on the phase distribution in a fully developed dispersed two-phase flow. Liu [4] showed experimentally that the bubble size had effects on the void fraction distribution and on the developing length of bubbly-to-slug flow transition. Nonetheless, those studies did not measure the local bubble sizes or an equivalent term—the interfacial area concentration. In our experimental study, distributions of void fraction and interfacial area concentration were measured by the resistivity probe method.

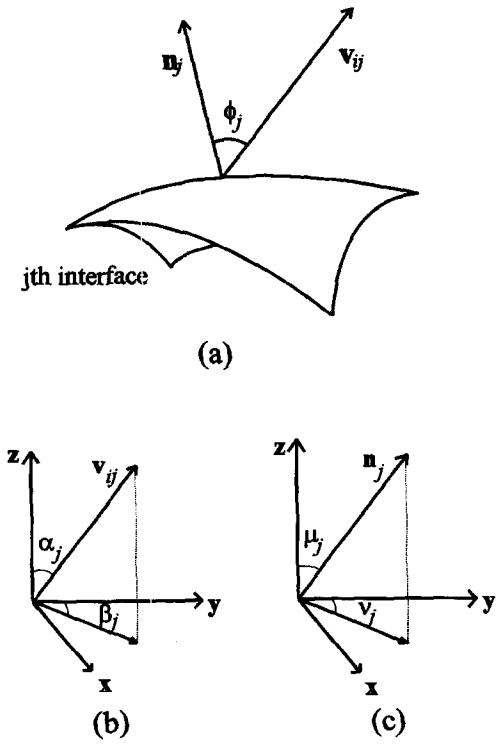

Fig. 1. (a) Double-sensor probe and jth interface. (b) Vector angles of $\mathbf{v}_{ij}$. (c) Vector angles of $\mathbf{n}_j$.

2. LOCAL INTERFACIAL AREA CONCENTRATION MEASUREMENT

As the name implies, the interfacial area concentration is defined as the average surface area within a unit volume. If it is defined at an arbitrary point in a two-phase mixture, the local instant interfacial area concentration is in the form of the delta function [5], which is not observable by any experimental means. Using the local instantaneous formulation, Kataoka *et al.* [5], derived the time average local interfacial area concentration equation in terms of observable parameters, and it is given as [5]:

$$\bar{a}_i^j(x,y,z) = \frac{1}{\tau}\overline{\frac{1}{|\mathbf{v}_i|\cos\phi}}, \tag{6}$$

where $\mathbf{v}_{ij}$ and ϕ_j are the interfacial velocity of jth interface and the angle between the velocity and the unit normal of the jth interface as shown in Fig. 1(a). The overbar denotes the arithmetic mean of the enclosed function and τ is the average time that the interface passes a given point. If the number of bubbles which pass the probe sensor per unit time is N_t, τ can be expressed as $\tau = 1/2N_t$. The factor 2 indicates that each bubble has two interfaces associated with it. Thus, the time averaged interfacial area concentration can be obtained by counting N_t and measuring $|\mathbf{v}_{ij}|\cos\phi_j$ for each interface. The velocity vector is characterized by the magnitude of the velocity, $|\mathbf{v}_{ij}|$, the zenithal angle, α_j, and the azimuthal angle, β_j [see Fig. 1(b)]. The unit outward normal of the jth interface has the magnitude of unity. The zenithal angle, μ_j, and the azimuthal angle v_j, are in the coordinate system where the velocity vector is defined [see Fig. 1(c)]. The dot product of $\mathbf{v}_{ij}$ and $\mathbf{n}_j$ can be expressed as:

$$|\mathbf{v}_{ij}|\cos\phi_j = |\mathbf{v}_{ij}|[\cos\alpha_j\cos\mu_j + \sin\alpha_j\sin\mu_j\cos(\beta_j - v_j)], \tag{7}$$

which is the normal velocity of the jth interface.

Assuming that there is no statistical correlation between $\mathbf{v}_{ij}$ and $\mathbf{n}_j$, which means that the velocity vector is not determined by the orientation of the interface or vice versa, the mean value of the velocity and the angles can be evaluated independently. If the number of samples is large, the summation can be approximated by an integration. Then $\cos\phi_j$ can be described by a continuous probability density function $P(\alpha,\beta,\mu,v)$. The harmonic mean of the normal interfacial velocity can be expressed as:

$$\overline{\frac{1}{|\mathbf{v}_i|\cos\phi}} = \overline{\frac{1}{|\mathbf{v}_i|}}\iiiint \times \frac{P(\alpha,\beta,\mu,v)\,d\alpha\,d\beta\,d\mu\,dv}{[\cos\alpha\cos\mu + \sin\alpha\sin\mu\cos(\beta - v)]}. \tag{8}$$

For simplicity, consider a homogeneous bubbly flow in an infinite medium, which means there is no spatial distribution of bubble number density, void fraction and bubble velocity. The bubble shape is assumed to be quasi-spherical. In addition, consider the flow is in the z-direction (i.e. the transverse bubble velocity is relatively small). Let $g(\alpha)$ be the probability distribution function of α. Based on a homogeneous model, $g(\alpha)$ has equal probability between 0 and α_0 (i.e. $g(\alpha) = 1/\alpha_0$ for $0 \leqslant \alpha \leqslant \alpha_0$, where α_0 is the maximum zenithal angle of the velocity vector and $0 \leqslant \alpha_0 \leqslant \pi/2$). The angle β takes on any value between 0 and 2π with equal probability because it does not have any preference in the azimuthal direction. For the statistical characteristic of $P(\mu, v)$, the probability to access a spherical surface in the azimuthal direction should be equal for $0 \leqslant \mu \leqslant 2\pi$, and the zenithal distribution is governed by the view factor of the sphere's surface from the pole. Then the overall probability density function can be written as:

$$P(\alpha,\beta,\mu,v) = \frac{1}{\pi}g(\alpha)\sin\mu\cos\mu\,d\alpha\,d\mu\,d(\beta - v). \tag{9}$$

Let $\mathbf{n}_s$ be the unit vector of the double-sensor probe: it makes an angle ξ_{ij} with the unit normal of jth interface $\mathbf{n}_j$. Let Δs be the separation of two sensors, and Δt_j be the time lapse for jth interface passing through both sensors, then the measured velocity, $\mathbf{v}_{sj}$, is equal to $\Delta s/\Delta t_j$. The relation between the measured velocity and the normal interface velocity of the jth interface is $|\mathbf{v}_{sj}|\cos\xi_j = |\mathbf{v}_{ij}|\cos\phi_j$. Furthermore, if $\mathbf{n}_s$ is aligned with the z-axis and the measured interfacial velocity becomes $\mathbf{v}_{szj}$, the relation of the angle cosines is

$\cos\xi_j = \cos\phi_j$. Based on the above considerations and substituting equation (8) into equation (6), we get:

$$\bar{a}_i^t(x,y,z) = 2N_t\left(\sum_j \frac{1}{|\mathbf{v}_{szj}|}\right) \times \frac{\int\int\int\int \frac{P(\alpha,\beta,\mu,v)\,d\alpha\,d\beta\,d\mu\,dv}{[\cos\alpha\cos\mu+\sin\alpha\sin\mu\cos(\beta-v)]}}{\int\int\int \frac{P(\alpha,\beta,\mu,v)\cos\mu\,d\alpha\,d\beta\,d\mu\,dv}{[\cos\alpha\cos\mu+\sin\alpha\sin\mu\cos(\beta-v)]}}. \quad (10)$$

The integration limits are $0 \leqslant \alpha \leqslant \alpha_0$, $0 \leqslant \mu \leqslant \pi/2$, and $0 \leqslant \beta, v \leqslant 2\pi$. Substituting the probability function defined in equation (9) and integrating over the limits, the following result is obtained [5]:

$$\bar{a}_i^t(x,y,z) = \frac{4N_t\sum_j \frac{1}{|\mathbf{v}_{szj}|}}{1-\cot\frac{\alpha_0}{2}\ln\left(\cos\frac{\alpha_0}{2}\right)-\tan\frac{\alpha_0}{2}\ln\left(\sin\frac{\alpha_0}{2}\right)}. \quad (11)$$

Therefore, the time averaged local interfacial area concentration can be obtained if values of $\mathbf{v}_{szj}$, N_t and α_0 are known. The velocity, v_{szj}, and the bubble number frequency, N_t, are obtained directly from the experimental measurements. The angle, α_0, is estimated from the statistical parameters of the measured interfacial velocity. The random fluctuation of the liquid phase turbulence causes the lateral motion of the bubbles which is assumed to be isotropic. The angle, α_0, can be formulated in terms of the statistical characteristics of the axial velocity [5]:

$$\frac{\sin 2\alpha_0}{2\alpha_0} = \frac{1-(\sigma_z^2/|\mathbf{v}_{iz}|^2)}{1+3(\sigma_z^2/|\mathbf{v}_{iz}|^2)}, \quad (12)$$

where σ_z is the standard deviation of the measured $\mathbf{v}_{iz}$. Knowing the average velocity in the z-direction and the standard deviation, α_0 can be determined. Then the time averaged local interfacial area concentration can be calculated using the relations given by equation (11). A more detailed derivation of the local interfacial area concentration measurement method was discussed by Kataoka *et al.* [5].

3. DOUBLE-SENSOR PROBE AND LOCAL MEASUREMENT METHODS

The time averaged local interfacial area concentration can be evaluated from statistical parameters of the bubble velocity and the bubble number frequency. A dual-sensor resistivity probe is best suited for this task. The phase sensing principle of the probe is based on the instantaneous conductivity of the surrounding media. Voltage signals are obtained from the nodes across the sensors and the ground. Since the sensors make electrical contact with the surrounding liquid, they must be made of material which is highly conducting and electrochemically stable to the surrounding fluid. Furthermore, they must be strong enough to withstand the flow and the shock of interface pinching. In addition, the sensor diameter must be small and the probe must be miniaturized to avoid interface distortion during the measurement. These are some of the criteria used for constructing a resistivity probe.

3.1. *The double-sensor probe method*

The probes were made of a 0.12 mm diameter platinum/rhodium (13%) wire. The sensor wire was insulated with a varnish resin and then inserted into a small stainless steel tube. The varnish resin was used to seal and bond the tubes together. The distance between the upstream and downstream sensors was 2–4 mm. The insulation on the sensor-tip was stripped away to expose the metal wire, and the exposed length was roughly 2–3 times that of the wire diameter. The other end of the sensor was soldered to a copper wire lead which would be connected to the biasing circuit. The probe assembly was bonded to a 3.175 mm o.d. holder tube which had a 90° elbow bend.

The probe was inserted into the test section from the side wall and supported by a metal holder mounted on the outer wall of the test section. A micrometer was attached to the probe holder and was used to traverse the probe in the radial direction. A 5-V d.c. power supply was used for the biasing and an adjustable resistor was connected in series with the sensor. The biasing resistor was adjusted to give an optimum output voltage for measurements. If the sensor is in a liquid phase, the circuit will be closed and the voltage output will be lower. When a gas bubble hits the sensor, the circuit continuity will be broken and the output will read a higher voltage.

The probe signals were digitized by a fast A–D converter, MetraByte DAS-20, and were stored in a DELL-325 personal computer. The sampling rate of the data acquisition was set at 10 kHz per channel. At this sampling rate the measurement error of the velocity is less than 5% if the distance between the sensors is greater than 2 mm. The total sampling time was 75 s in order to get enough bubbles for computing the statistical characteristics of the interfacial velocity. On average, 1500–4000 bubbles were detected in each sample of raw data.

3.2. *Signal processing*

Since the double probe sensors are separated by a finite distance and a bubble is free to move in any direction, a bubble that hits the upstream sensor is not always intercepted by the downstream sensor or vice versa. The non-associated signals from both sensors produce errors in the velocity measurement. In order to ensure that the downstream sensor indeed detects the same interface which hit the upstream sensor, the following criteria were used for the signal processing;

1. *minimum waiting time*—when the fastest bubble

hits the upstream sensor, it takes the shortest time to reach the downstream sensor;
2. *maximum waiting time*—when the slowest bubble hits the upstream sensor, it takes the longest time to reach the downstream sensor; and
3. *compatible resident time*—the resident time of a bubble in the upstream sensor and in the downstream sensor should be compatible and the time difference should be less than 30%.

A higher output voltage indicates that the sensor dwells in the gas phase and a lower output voltage indicates that the sensor dwells in the liquid phase. The rising and falling edges of these pulses mark the interfaces. The time averaged local void fraction is determined by the fraction of time that the sensor spends in the gas phase over the total sampling time. Let t_{urj} be the instant that jth bubble front interface hits the upstream sensor and t_{ufj} be the instant that the rear interface of jth bubble leaves the upstream sensor. Let $\Delta\tau_j$ denote the time duration of the upstream sensor spending in jth bubble, then $\Delta\tau_j = |t_{ufj} - t_{urj}|$. If Ω is the total sampling time and N_t is the total number of bubbles detected by the upstream sensor, the time averaged local void fraction is given as:

$$\alpha(x_0, y_0, z_0) = \frac{1}{\Omega} \sum_{j=1}^{N_t} \Delta\tau_j, \tag{13}$$

where x_0, y_0 and z_0 are the coordinates of the upstream sensor. Only the upstream sensor signal is used for evaluating the local void fraction. The downstream sensor usually gives a lower value of void fraction because the upstream sensor may affect the bubble reaching the downstream sensor.

Let Δs be the distance between the upstream and the downstream sensor. The sensors are in line with the z-axis. Let t_{drj} be the instant that the front interface of the jth bubble hits the downstream sensor. Let Δt_j denote the time lapse of the jth interface traveling from the upstream sensor to the downstream sensor and it is given as $\Delta t_j = |t_{drj} - t_{urj}|$. Let N_{tv} be the total number of bubbles hitting both the upstream and downstream sensor (noticing that $N_{tv} < N_t$), then the mean of the axial velocity is:

$$\overline{|v_{iz}|} = \frac{1}{N_{tv}} \sum_{j=1}^{N_{tv}} \frac{\Delta s}{\Delta t_j}. \tag{14}$$

The harmonic mean of the axial velocity and the root mean square of axial velocity fluctuation can be calculated accordingly. In view of equation (11), the interfacial area concentration can be evaluated if the bubble number frequency and the statistical characteristics of the axial interfacial velocity are known.

4. THE EXPERIMENTAL APPARATUS

A schematic diagram of the air–water loop is shown in Fig. 2. The test section is made of an extruded Lucite tube 5.08 cm i.d. and 375 cm long. In this paper, the authors consider the upward co-current vertical flow. Water is injected into the mixing chamber where the bubble generator is located. A centrifugal pump provides a constant pressure head for the forced flow. The flow rate is controlled with a bypass flow and a globe value. The maximum flow rate obtained with this pump is 1 m s^{-1} in a 5.08 cm i.d. pipe. The bubble generator is made of a sintered stainless steel tube of 2.54 cm o.d. with a porous wall length 5 cm; the pore size is 40 μm. Air is injected through the lower chamber from a large pressurized storage tank. The chamber acts as a buffer to avoid any sudden pressure fluctuation. Bubbles are grown on the porous wall and are sheared off by the water flow in the mixing chamber. After mixing together as a two-phase fluid, the mixture flows upward through a short convergent section into the test section.

5. EXPERIMENTAL RESULTS AND DISCUSSION

Experimental studies were performed on the dispersed bubbly flow regime with the air–water system. Data were acquired at two axial locations; $L/D = 8$ and $L/D = 60$. The first location represents the entrance region and the second location represents the fully developed region. A double-sensor resistivity probe was employed for measuring the time averaged local void fraction, interfacial velocity, and bubble frequency. Four different liquid flow rates in combination with four different gas injection rates were studied. They were:

1. superficial liquid velocity:
   $j_l = 1.0, 0.6, 0.4, 0.1$ m s^{-1}; and
2. superficial gas velocity:
   $j_g = 0.0965, 0.0696, 0.0384, 0.0192$ m s^{-1}.

With these experimental conditions, the void fraction ranged from 2.4 to 27%, which was in the bubbly flow regime.

5.1. *Measurement error*

The error of the local measurements can be estimated according to the basic uncertainties in the measurement technique:

1. sensor tip wetting characteristics; and
2. electronic circuit response and data acquisition.

The first error was minimized by choosing a proper threshold level on the probe signal. The maximum error resulted from this procedure was less than 4% on the void fraction measurement. The second error, due to the electronic circuit response and the data acquisition system, was about 2.5%. The total error on the void fraction was about 7%. The error of interfacial area concentration estimation was about 9%. The error due to dynamics of the flow is a separate error which depends on the flow. In the measurements, a long sampling time (75 s) was taken to minimize the dynamic error. In the present case the typical dynamic error in the measurement of the void fraction was 2%.

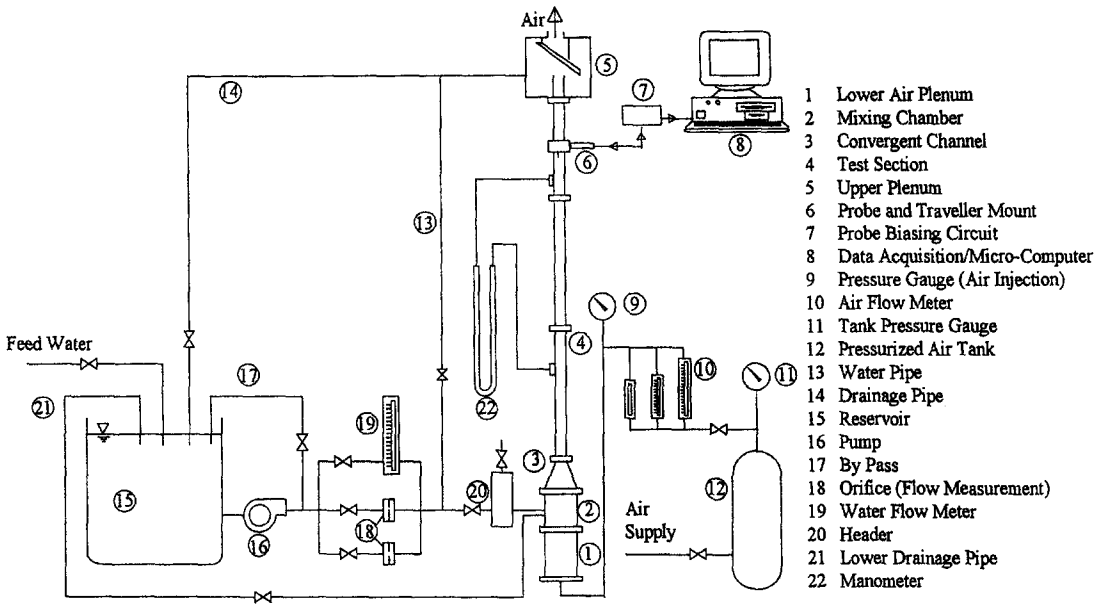

Fig. 2. The air–water loop schematic.

The error of the overall void fraction and interfacial area concentration can be obtained by comparing the probe measurements with the standard methods. A two-phase pressure drop measurement was used for the void fraction comparison and a photographic method was used for the interfacial area concentration comparison. Figure 3 shows the comparison of the cross-sectional average void fraction by the probe method and by the pressure drop measurements. The frictional pressure drop was calculated by the homogeneous model. Most of the data were within a 20% error range compared to the pressure drop measurement. The photographic study is a time consuming method and it can be used only for low void fraction mixture (less than 10%). Hence, the result is simply a quote from the authors' previous study [6] for the overall error estimation. The calibration studies were conducted in the same experimental set-up used in the current study. The result should be similar to the present work. Figure 4 shows the comparison plot of such a result. The probe data were within a 20% error compared to the photographic study.

The overall error is much larger than the estimated error in the local measurement. The main reason is that the void fraction distribution may not be axially symmetric. Since we have measured in one azimuthal direction only, the magnitude may be lower or higher than the average values at each radial point. Nevertheless, the shape of the profile and the characteristics of the flow should be similar in all azimuthal directions.

5.2. *The local profile characteristics*

For this discussion, the data illustrating the characteristic profile changes in the developing flow are con-

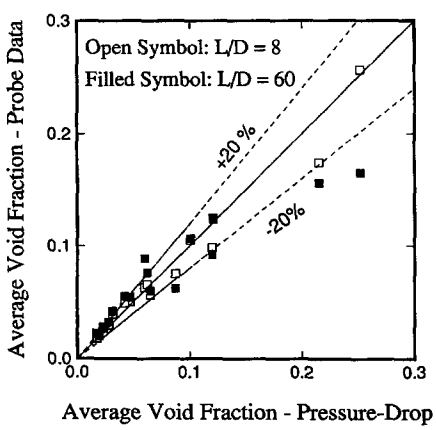

Fig. 3. Comparison of average void fraction data from double-probe and pressure-drop measurements.

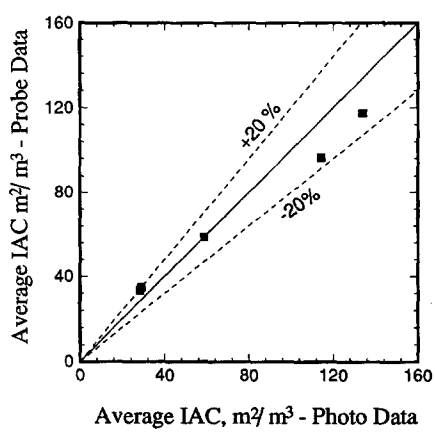

Fig. 4. Comparison of average interfacial area concentration data from double-sensor probe and photographic measurements (from Ishii and Revankar [6]).

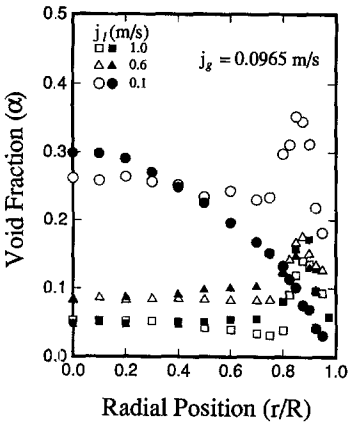

Fig. 5. The radial profiles of void fraction (open symbol: $L/D = 8$, and filled symbol: $L/D = 60$).

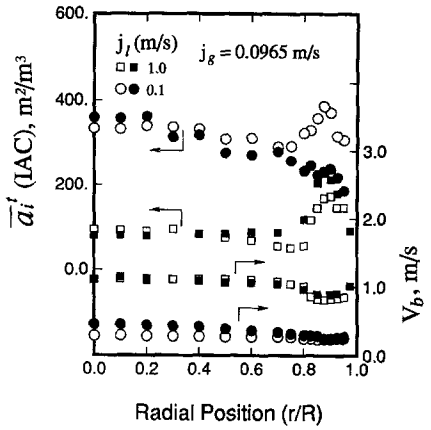

Fig. 6. The radial profile of interfacial area concentration and bubble velocity (open symbol: $L/D = 8$, and filled symbol: $L/D = 60$).

sidered. The full set of the local data can be found in Leung *et al.* [7], and the detailed local profile comparison can be found in Ishii *et al.* [8]. In Figs. 5–7, the radial profile of void fraction, interfacial area concentration, bubble velocity, bubble frequency and Sauter mean diameter are shown, and the data at both the entrance and fully developed regions are compared. The radial void fraction profiles are shown in Fig. 5, for $j_l = 1.0, 0.6$ and 0.1 m s^{-1} with $j_g = 0.0965$ m s^{-1}. At the entrance region ($L/D = 8$), all the radial profiles show a bubbly flow distribution with the void fraction peaks near the pipe wall. The local void fraction begins to rise at roughly $r/R = 0.78$, which is 5.6 mm from the pipe wall. This spacing is roughly 1.5 times the typical bubble size (3.7 mm). At the core region ($r/R < 0.75$), the void profiles are close to a parabolic shape. At the fully developed region, the void distribution is flat across the core and has a near wall peak for the cases of $j_l = 1.0$ and 0.6 m s^{-1}, showing very little change in void distribution from the entrance to the fully developed region.

Zun *et al.* [9] have found, through their experimental data and numerical calculations, that the bubble segregation process is achieved within a distance of $L/D = 10$. An equilibrium profile maintains its form for a long distance from the entrance. In the authors' experiments, the void distribution shows a wall void peak established a short distance from the entrance. The phase distribution does not change along the axial direction for the cases $j_l = 1.0$ and 0.6 m s^{-1}. Liu [4] also has a similar observation on the void profile development. In the case of $j_l = 0.1$ m s^{-1}, however, the void profile becomes parabolic at $L/D = 60$, which is a significant change from the entrance region where a wall peak is observed.

The profile shape of the interfacial area concentration is similar to its void fraction profile, so only two cases of radial distributions are shown in Fig. 6 to illustrate this point. Comparing the profiles between two stations, the profiles evolve in the same way as their void fraction counterparts. In other words, the gas phase remained as dispersed bubbles in all the cases. In the case of $j_l = 0.1$ m s^{-1}, the interfacial area concentration distribution with a near wall peak at $L/D = 8$ changed to a parabolic distribution at $L/D = 60$. The high interfacial area concentration at the developed region indicated that the gas phase remained as separated bubbles without much coalescence even though the flow was close to regime transition.

The radial bubble velocity profiles are also presented in Fig. 6. For the case of $j_l > 0.1$ m s^{-1}, the measured bubble velocities are close to the values predicted by the drift flux model [10]. The velocity profile is flat across the core region, and it decreases sharply near the wall ($r/R = 0.78$). The magnitude of the decrease depends on the superficial liquid velocity (as much as 20 cm s^{-1} for $j_l = 1.0$ m s^{-1}). It tends to smooth out at the fully developed region. Comparing velocities measured at two axial locations, there is no appreciable change at the core region. The bubbles reach their terminal velocities in a very short distance from the entrance. For the case of $j_l = 0.1$ m s^{-1}, the bubble velocity decreases smoothly at the wall. At the fully developed region, however, the centerline bubble velocity increases to 0.45 from 0.28 m s^{-1} at the entrance, and the velocity profile becomes more parabolic.

Based on Figs. 5 and 6 (the void fraction and interfacial area profiles), we conclude that the near wall void peak is due to the higher concentration of bubbles. In order to verify this point, both the bubble frequency and the Sauter mean diameter are plotted in Fig. 7 for the same cases of j_ls and j_g. The bubble frequency distributions are directly proportional to the void fraction; higher bubble frequency for higher void fraction and vice versa. The profiles of the Sauter mean diameter are also plotted in the same figure. The average bubble size is 3.8 mm in the core region and it increases to 5 mm near the pipe wall. A similar observation was reported by Liu [4], and he asserted

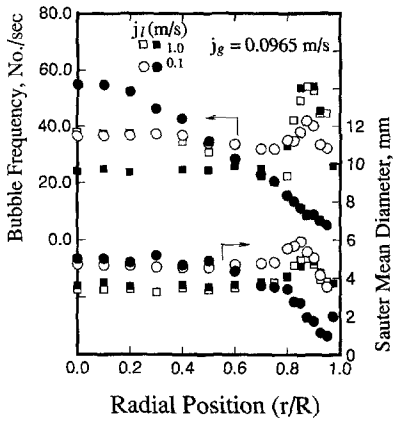

Fig. 7. The radial profiles of bubble frequency and Sauter mean diameter (open symbol: $L/D = 8$, and filled symbol: $L/D = 60$).

that the possible explanation was either due to coalescence or due to bubbles stretching in a shear field. However, the authors think that the larger mean diameter measured at the wall region is due to measurement error. The isotropic velocity fluctuation assumption is not valid near the pipe wall and, hence, the interfacial area concentration measurement becomes inaccurate.

5.3. *The average characteristics*

The void fraction is assumed to be evenly distributed in the azimuthal direction. The pipe area is divided into concentric rings according to the radial position of the local measurements. The area average parameters are obtained by multiplying the local parameters by the area ratio and summing them together. In analyzing the averaged data, the drift flux presentation is an appropriate method. The correlation equation is given by Zuber and Findlay [11]:

$$\frac{\langle j_g \rangle}{\langle \alpha \rangle} = C_0 \langle j \rangle + V_{gj}, \tag{15}$$

where j_g, j, C_0, and V_{gj} are the superficial gas velocity, total volumetric flux, distribution parameter, and drift velocity, respectively. The angle parenthesis denotes an area averaged value of the parameter enclosed.

In Fig. 8, the area averaged gas velocity is plotted against total volumetric flux. The slope gives the value of C_0 and the y-interception gives the drift velocity, V_{gj}. The recommended value for C_0 is 1.2 for fully developed bubbly flow in a round pipe [12]. However, the best fit of the experimental data gives the value of C_0 between 0.6 and 0.8. This is expected because most of the void fraction profiles are saddle shaped. The drift velocity, V_{gj}, is found to be 20 cm s^{-1} from this plot.

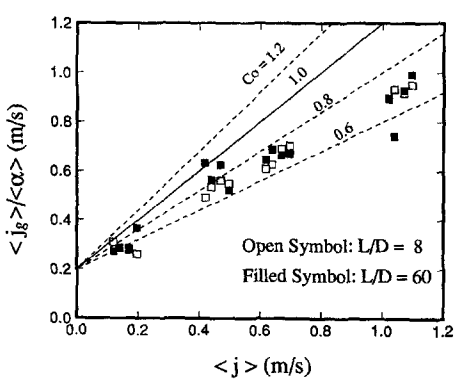

Fig. 8. The drift flux plot.

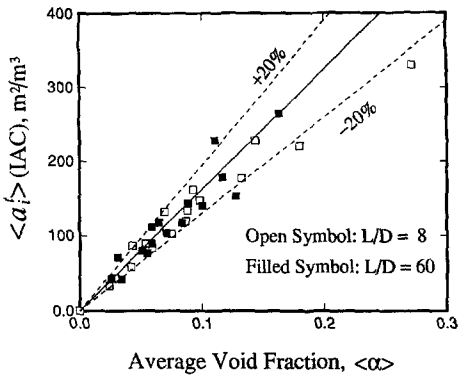

Fig. 9. The average interfacial area concentration vs the average void fraction.

In Fig. 9, the area averaged interfacial area concentration is plotted against the area averaged void fraction. The Sauter mean diameter is inversely proportional to the average slope of the plot. A straight line was drawn through the data points such that all the points are scattered within $\pm 20\%$. The averaged Sauter mean diameter obtained by this method is 3.7 mm, which agrees with our previous studies [6, 13]. The data are expected to be scattered more severely in the high void fraction cases because the statistical characteristics of bubble motion change at the flow regime transition. However, the present area averaged data do not show much scatter. For the high void fraction cases, at the entrance region, the interfacial area concentration data points bend below the average line. This indicates that the bubble size is larger to start with in the low velocity higher void fraction case.

In Fig. 10, the normalized void peak ($\alpha_{peak}/\langle\alpha\rangle$) vs

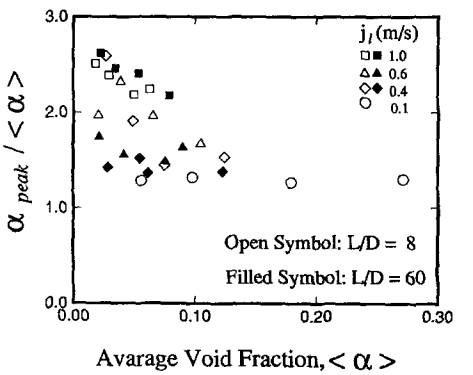

Fig. 10. The normalized void peak vs the average void fraction.

the averaged void fractions are plotted. At the entrance region, the void peak strongly depends on the average void fraction regardless of the liquid volumetric flow rate. The void peak decreases as the averaged void fraction increases. The normalized void peak ranges from 2.5 to 1.5 for all cases. For the case of $j_l = 0.1$ m s^{-1}, the normalized peak is equal to 1.3 regardless of the averaged void fraction. In the fully developed region, the normalized peak decreases for the cases of $j_l = 0.4$ and 0.6 m s^{-1} and is less dependent on the averaged void fraction. For the case of $j_l = 1.0$ m s^{-1}, the normalized void peak at the developed region is higher than that at the entrance region.

6. CONCLUSION

The double-sensor probe method for measuring time average local interfacial area concentration in a dispersed bubbly flow has been described. In the dispersed bubbly flow, the fluctuation of the bubble velocity is isotropic. As a result, the transverse-direction velocity-component can be estimated from the root mean square of the axial velocity fluctuation. Using the double-sensor probe, data were obtained on the local void fraction and interfacial area concentration profile at two locations of the test section: the entrance region ($L/D = 8$) and the fully developed region ($L/D = 60$). These data sets are particularly useful in understanding the development of bubbly flow in tubes.

At the entrance region of the test section, the near wall void peak is observed for all the cases of flow rate studies. In the fully developed region ($L/D = 60$), the near wall void peak is higher in the case of $j_l = 1.0$ m s^{-1}, and it is lower in the cases of $j_l = 0.6$ and 0.4 m s^{-1} compared to the one at the entrance region. In the case of $j_l = 0.1$ m s^{-1}, the radial void fraction profile changes from a wall peak to a parabolic distribution as the flow develops from the entrance region to the fully developed region. The local profiles of the bubble frequency and interfacial area concentration follow the void fraction profile behavior very closely at both the entrance and the fully developed regions.

The one-dimensional analysis of the averaging flow quantities is presented by the drift flux plot. We find that the distribution parameter, C_0, is equal to 0.7 which is consistent with the near wall void peak observation. The area averaged interfacial area concentration increases linearly with the averaged void fraction. This indicates that the two-phase mixture remains in the bubbly flow regime. The averaged Sauter mean diameter obtained is 3.7 mm.

Acknowledgments—This work was performed under the auspices of the U.S. Department of Energy, Office of Basic Energy Science. The authors would like to express their sincere appreciation for the encouragement, support and the technical comments on this program from Dr O. P. Manley of DOE/BES.

REFERENCES

1. M. Ishii, *Thermo-Fluid Dynamic Theory of Two-Phase Flow*. Eyrolles, Paris, or Scientific and Medical Publication of France, NY (1975).
2. M. Ishii and K. Mishima, Two-fluid model and hydrodynamic constitutive relations, *Nucl Engng Design* **82,** 107–126 (1984).
3. A. Serizawa, I. Kataoka, A. Gafuku, O. Takahashi and Z. Kawara, Bubble size effect on the flow structure. *Proceedings of the International Conference on Multiphase Flow*, Tsukuba, Japan, pp. 547–550 (1991).
4. T. J. Liu, Bubble size and entrance length effects on void development in a vertical channel, *Int. J. Multiphase Flow* **19,** 99–113 (1993).
5. I. Kataoka, M. Ishii and A. Serizawa, Local formulation of interfacial area concentration in two-phase flow, *Int. J. Multiphase Flow* **12,** 505–529 (1986).
6. M. Ishii and S. T. Revankar, Local interfacial area measurement in bubbly flow, Argonne National Laboratory Report, ANL-90/51 (1991).
7. W. H. Leung, S. T. Revankar, Y. Ishii and M. Ishii, Interfacial area and two-phase flow structure development measured by double-sensor probes, Purdue University Report, PU NE-92/1 (1992).
8. M. Ishii, S. T. Revankar and W. H. Leung, Multi-sensor probe method for local measurement of two-phase flow characteristics. *U.S.–Japan Seminar on Two-Phase Flow Dynamics*, Berkeley, CA (1992).
9. I. Zun, I. Kljenak and S. Moze, Space–time evolution of the nonhomogeneous bubble distribution in upward flow, *Int. J. Multiphase Flow* **19,** 151–172 (1993).
10. M. Ishii, T. C. Chawla and N. Zuber, Constitutive equation for vapor drift velocity in two-phase annular flow, *A.I.Ch.E. Jl* **22,** 283–291 (1976).
11. N. Zuber and J. A. Findlay, Average volumetric concentration in two-phase flow systems, *J. Heat Transfer* **87,** 453–468 (1965).
12. M. Ishii, One-dimensional drift-flux model and constitutive equations for relative motion between phases in various two-phase flow regimes, Argonne National Laboratory Report, ANL-77-47 (1977).
13. S. T. Revankar and M. Ishii, Local interfacial area measurement in bubbly flow, *Int. J. Heat Mass Transfer* **35,** 913–925 (1992).